INSPYRE
Investigations Supporting MOX Fuel Licensing in ESNII Prototype Reactors

EERA JPNM
JOINT PROGRAMME ON NUCLEAR MATERIALS

D7.4 - Results of the applicative benchmark between TRANSURANUS and GERMINAL on the ASTRID case study

B. Michel, M. Lainet (CEA), A. Magni, L. Luzzi, D. Pizzocri (POLIMI)

Version 1 – 31/07/2021

The INSPYRE project has received funding from the EURATOM research and training programme 2014-2018 under Grant Agreement No 754329.

Document type	Deliverable
Document number	D7.4 version 1
Document title	Results of the applicative benchmark between TRANSURANUS and GERMINAL on the ASTRID case study
Authors	B. Michel, M. Lainet (CEA), A. Magni, L. Luzzi, D. Pizzocri (POLIMI)
Release date	31/07/2021
Contributing partners	CEA, POLIMI
Dissemination level	Public

Version	Short description	Main author	WP leader	Coordinator
1	First release	B. Michel (CEA) 28/07/2021	L. Luzzi (POLIMI) 28/07/2021	M. Bertolus (CEA) 31/07/2021

SUMMARY

This deliverable addresses one of the benchmark activities foreseen in Task 7.3 of INSPYRE, which focuses on the simulation of irradiation case studies representative of the ESNII reactor prototypes. The goal of this work is to assess the predictive design capabilities of fuel performance codes before and after the improvements brought about by the INSPYRE Project.

The ASTRID case study, which was selected by the Task Force on fuel performance codes taking into account the needs expressed by the User Group, is a base irradiation for an axially heterogeneous fuel pin representative of the maximal loading condition in the ASTRID reactor.

This case study was analysed by POLIMI using the TRANSURANUS fuel performance code and by CEA using the GERMINAL code.

CONTENT

GLOSSARY

ASTRID	Advanced Sodium Technological Reactor for Industrial Demonstration
bfc	bottom of fuel column
CER	Cladding External Radius
CET	Cladding External Temperature
CHBS	Cladding Hoop Bending Stress
CHMS	Cladding Hoop Membrane Stress
CP	Contact Pressure
dpa	displacements per atom
efpd	equivalent full power days
EOL	End Of Life
FCT	Fuel Central Temperature
FGR	Fission Gas Release
FPIP	Fuel Pin Internal Pressure
FPIR	Fuel Pellet Inner Radius
FR	Fast Reactor
INSPYRE	Investigations Supporting MOX Fuel Licensing for ESNII Prototype Reactors
JOG	Joint Oxyde-Gaine
LHR	Linear Heat Rate
LWR	Light Water Reactor
O/M	Oxygen-to-Metal ratio
P2CG	Pellet-To-Cladding Gap
PCMI	Pellet-Cladding Mechanical Interaction
WP	Work Package

1 INTRODUCTION

The ASTRID fuel pin concept is based on a heterogeneous axial fuel column and annular pellets. Key criteria to be assessed under nominal irradiation are (1) the power-to-melting margin at the beginning of irradiation and (2) the cladding maximal hoop stress at the end of irradiation.

The main objective of the current benchmark between the TRANSURANUS and GERMINAL codes is to assess the behaviour of the hot channel fuel pin under nominal irradiation conditions and to discuss the impact of the modelling improvements done in the INSPYRE Project, which are presented in Deliverable D7.2 [1]. To this aim, the results of the pre-INSPYRE and post-INSPYRE versions ones are compared.

This document first describes the input data needed for the ASTRID benchmark and then presents the results yielded by the two fuel performance codes. Finally, the impact of the modelling improvements is discussed.

2 INPUT DATA

Table 1 reports the geometry of an inner core fuel pin representative of the ASTRID design [2]. The cladding material is an austenitic stainless steel 15-15Ti (15% Cr, 15% Ni, 0.45% Ti) and the fuel is made of plutonium-uranium mixed oxides. Figure 1 reports a schematic of the fuel pin section.

The considered nominal conditions correspond to ASTRID operating at 1500 MW_{th}. The sodium inlet temperature is assumed to be constant in time and equal to 400 °C, with a pressure of 0.3 MPa. The sodium mass flow rate per pin is also constant and equal to 0.1 kg/s. The pin-pitch is of 10.7 mm (9.7 mm of pin diameter and 1 mm of wire diameter).

The irradiation history considered ([3], shown in Figure 2) presents a maximum linear heat rate of q' = 463 W/cm at the beginning of irradiation. The fuel residence time is of 1440 efpd (equivalent full power days), divided in four cycles of 360 efpd each, with a progressive power decrease of 10% up to the end of the irradiation. The Linear Heat Rate evolution at the pin Peak Power Node is shown in Figure 2.

The total neutron flux φ is proportional to the linear heat rate, i.e., φ (n/cm^2-s) = 7.31 10^{12} q' (W/cm). As for the cladding damage, it is assumed that 70% of the flux has a neutron energy above 0.111 MeV, i.e., is considered as fast. The axial shape factor for both the linear heat rate and the flux is reported in Table 2 and in Figure 3 [4],[5].

Table 1: Geometry of the ASTRID fuel pin and fuel characteristics [6]. If not specified, variables concern both the fissile and the fertile pellets.

Variable	Value
Lower fertile zone height (mm)	300
Lower fissile zone height (mm)	250
Inner fertile zone height (mm)	200
Upper fissile zone height (mm)	350
Lower plenum length (mm)	800
Upper plenum length (mm)	80
Inner diameter, fissile pellet (mm)	2.45
Fuel outer diameter (mm)	8.46
Cladding inner diameter (mm)	8.70
Cladding outer diameter (mm)	9.70
Filling gas (He) pressure (MPa)	0.1
Fuel grain size (µm)	10
Porosity (%)	5
O/M, fissile pellet	1.97
O/M, fertile pellet [a]	2.00
Pu/M, fissile pellet [b]	0.23

[a] UO_2, U-nat.

[b] Pu-238/Pu = 0.23%, Pu-239/Pu = 67.87%, Pu-240/Pu = 26.07%, Pu-241/Pu = 4.62%, Pu-242/Pu = 1.2% (wt.%). U-nat.

Table 2: Axial profile of the pin linear power and fast neutron flux, based on [5].

Axial position (cm), from bfc	Shape factor (/)	Pellet type
104.17	0.8460	Fissile
92.50	0.9945	Fissile
80.83	0.9293	Fissile
70.00	0.0509	Fertile
60.00	0.0416	Fertile
50.83	0.5807	Fissile
42.50	0.5270	Fissile
34.17	0.4253	Fissile
25.00	0.0208	Fertile
15.00	0.0069	Fertile
5.00	0.000	Fertile

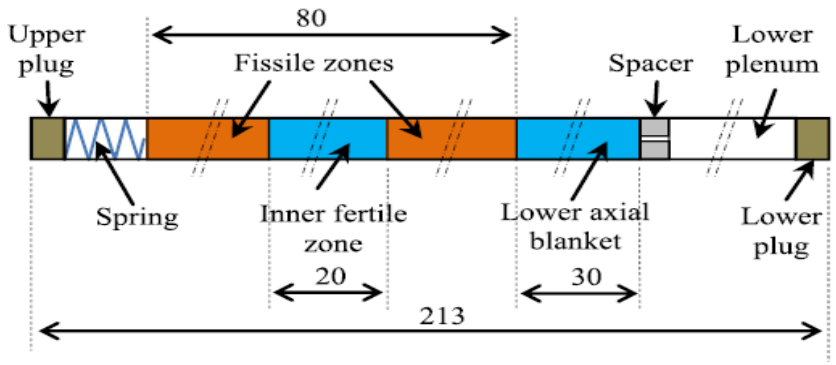

Figure 1: Schematic of an inner core ASTRID fuel pin (dimensions in cm) [6].

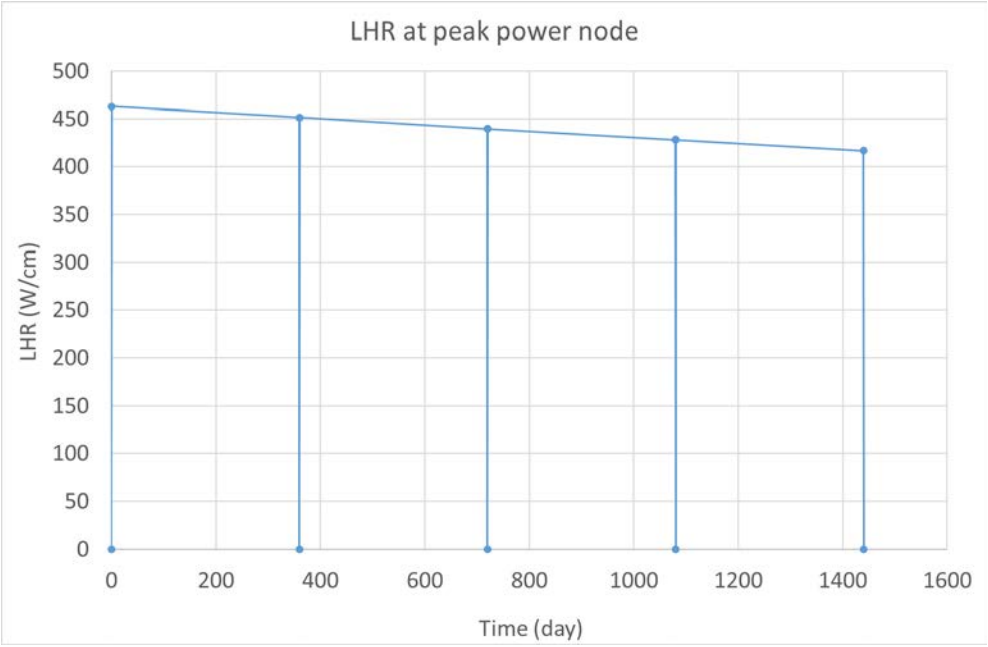

Figure 2: Linear Heat Rate evolution at the Peak Power Node.

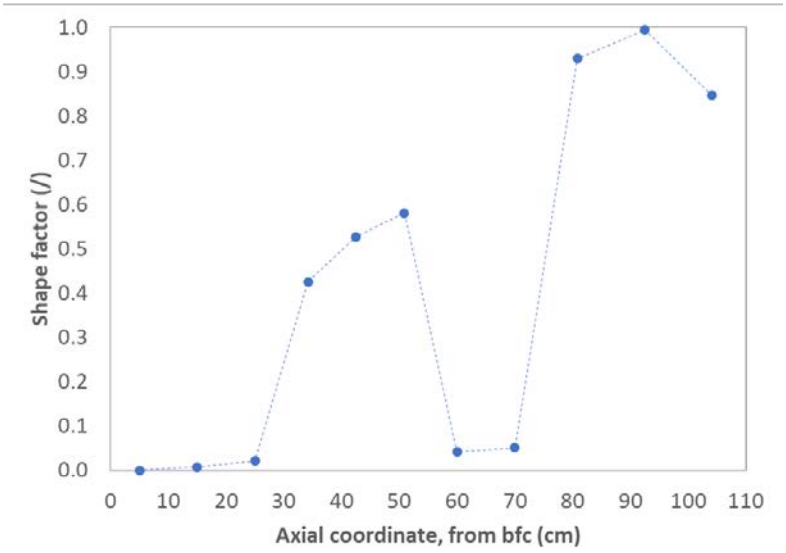

Figure 3: Graphical representation of the axial profile of the pin linear power and fast neutron flux, based on [5].

3 RESULTS

Results are given from Figure 4 to Figure 18 for GERMINAL (left) and TRANSURANUS (right). Each figure shows the initial reference results, labelled "pre-INSPYRE" (obtained from code versions prior to the models developed in INSPYRE), and the new results labelled "post-INSPYRE". The latter were obtained employing, in both GERMINAL and TRANSURANUS, novel property correlations and models according to the recommendations derived from the WP6 results, as specified in Deliverable D7.2 [1]. In the case of TRANSURANUS, three "post-INSPYRE" options were tested:

- "POST-INSPYRE" version: employing the novel recommendations for MOX thermal properties (thermal conductivity and melting temperature) [7], [8], MOX mechanical properties (Young's modulus and thermal expansion) [9] and the complete coupling with the SCIANTIX fission gas behaviour module [10].
- "POST-INSPYRE w/o grain growth": same settings of the "POST-INSPYRE" option, but without considering the fuel grain growth.
- "POST-INSPYRE w/o grain growth w/ conservative clad swelling": same settings as the "POST-INSPYRE" option, but without considering the fuel grain growth and employing the conservative correlation for the 15-15Ti swelling available in TRANSURANUS [11].

For GERMINAL the "post-INSPYRE" version includes the new recommendations for thermal and mechanical elastic properties. This version also includes some features of the SCIANTIX library for the release and swelling of Xe and Kr fission gases.

3.1 Peak Power Node results versus time

3.1.1 Fuel Central Temperature

3.1.1.1 Pre-INSPYRE results

The maximal temperature reached at the end of the first power increase is equal to 2280°C according to GERMINAL and 2105°C from TRANSURANUS calculations.

In the case of GERMINAL, the fuel central temperature (FCT) decreases rapidly at the beginning due to the fuel-cladding gap closure, then decreases slowly between 10 and 4500 hours due to the extension of the central hole induced by porosity migration. Then, the fuel conductivity and the gap conductance degradations lead to a temperature increase partially compensated by the beneficial effect of the O/M ratio increase and the power decrease. The sudden temperature decrease before the end of the second cycle is due to the JOG formation, which improves the fuel-cladding gap conductance.

As for TRANSURANUS results, the fuel central temperature (driven by fuel thermal conductivity, modelled with Philipponneau's correlation [12] for the fissile pellets and by fuel-cladding gap conductance) decreases significantly at beginning of life and during the first power cycle mainly due to strong fuel thermal expansion leading to fast gap size reduction (Figure 6). From the second irradiation cycle on, when the gap is closed, the central temperature tends to an almost constant value, due to a compensation between the degradation of fuel thermal conductivity with fuel burn-up and the beneficial effect of the O/M ratio increase towards fuel stoichiometry.

3.1.1.2 Post-INSPYRE results

For GERMINAL the maximal temperature reached at the end of the first power increase is the same with the post-INSPYRE options. Then, FCT evolution shows some slight differences with the post-INSPYRE options. These differences seem to be mainly due to modifications induced by the fission gas model for swelling and release.

The three simulation strategies with TRANSURANUS (i.e., involving all the novel INSPYRE models [1] and the two sensitivity studies on the fuel grain growth and cladding swelling) all reveal a sensibly lower fuel temperature reached as a consequence of the first power increase. The new maximal temperature is around 1930°C, due to the combined effect of a higher predicted thermal conductivity and a higher thermal expansion [9] causing faster gap closure. Switching off the fuel grain growth or employing the conservative cladding swelling correlation both determine a higher fuel temperature regime during the intermediate cycles, due to e.g., a higher amount of intra-granular fission gas release in the first case (while the fuel-cladding gap is anyway closed, as shown by Figure 6). Nevertheless, the maximum fuel central temperature, reached at the beginning of the second power cycle, is slightly above 2000°C. The "post-INSPYRE" simulation strategies all lead to a higher temperature at the end of irradiation, i.e., 1970°C compared to 1760°C from pre-INSPYRE code version.

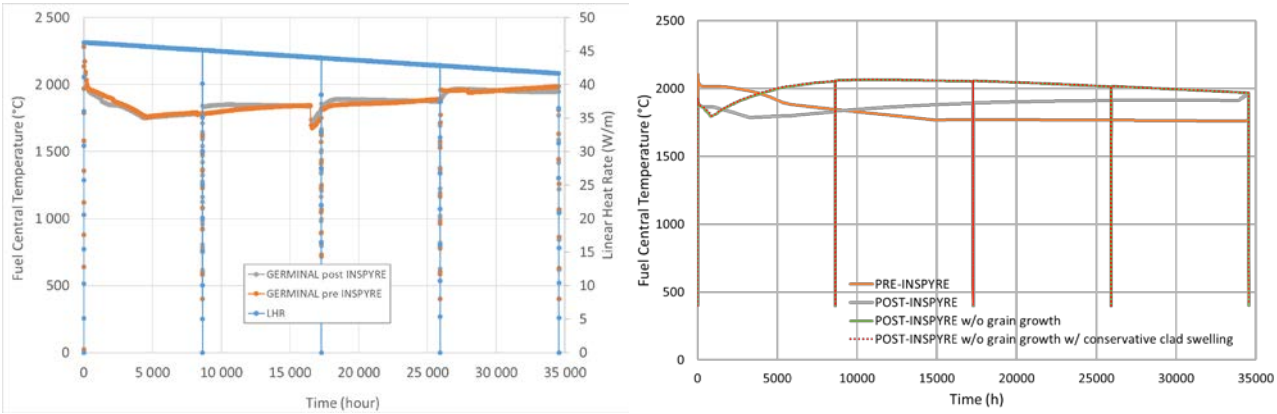

Figure 4: Fuel Central Temperature evolution at the Peak Power Node, as predicted by GERMINAL (left) and TRANSURANUS (right).

3.1.2 Fuel Pellet Inner Radius

3.1.2.1 Pre-INSPYRE results

The initial annular pellet experiences a radius increase due to porosity migration in both cases. The fuel pellet inner radius (FPIR) increases from 1.225 mm (as-fabricated value) to 1.56 mm for GERMINAL and to 1.42 mm from TRANSURANUS calculations. As discussed before, the significant inner radius increase before 4500 h explains the FCT decrease for GERMINAL, while TRANSURANUS predicts a slower evolution of the fuel inner radius. In the latter case, fuel restructuring is not deemed as the main phenomenon governing the fuel temperature evolution.

3.1.2.2 Post-INSPYRE results

For GERMINAL the FPIR evolution is a little different during the first 5000 h. These differences are probably linked to some yield effects associated to discrete (element by element) inner radius evolution in the GERMINAL model. After 5000 h the FPIR size tends to decrease slightly unlike the pre-INSPYRE results. This difference is probably linked to the fission gas model with an increase of the gaseous swelling, which tends to reduce the FIR in a situation where the gap is closed and the volume expansion can be accommodated by opened cracks in the pellet.

The fuel inner radius evolution predicted by TRANSURANUS POST-INSPYR" version is similar to the pre-INSPYRE one, despite a generally lower predicted fuel inner radius (its end-of-irradiation value is below 1.4 mm). On the contrary, the sensitivity simulations show that, the inner radius dynamics is visibly different. The post-INSPYRE results are almost identical whether the fuel grain growth model is turned on or off or the conservative correlation for cladding swelling is employed, and show a much slower increase of the fuel inner radius up to higher final values (~ 1.62 mm). A higher extent of fuel restructuring is promoted in these cases by the higher fuel temperature regime predicted from the end of the first cycle on, as reported in Figure 4. In addition, an enhanced fuel swelling caused by grain boundary bubbles plays a role on the fuel radial geometry. Switching off the fuel grain growth model means smaller grains releasing their fission gas inventory at grain boundaries, determining bigger inter-granular bubbles associated to a higher fuel swelling.

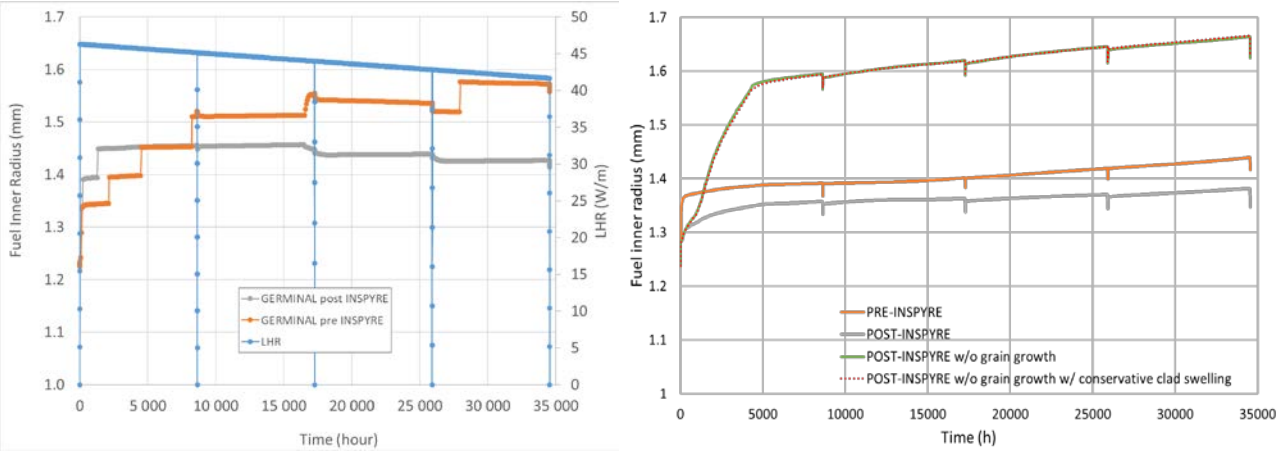

Figure 5: Fuel Pellet Inner Radius evolution at the Peak Power Node, as predicted by GERMINAL (left) and TRANSURANUS (right).

3.1.3 Pellet-To-Cladding Gap

3.1.3.1 Pre-INSPYRE results

In GERMINAL the pellet-to-cladding gap (P2CG) is closed 400 h after the initial power increase. Then, after 16000 h of irradiation, the gap reopens due to formation of the JOG, which is considered as a third material between the fuel and the cladding.

TRANSURANUS predicts instead a slower fuel-cladding gap closure during the first irradiation cycle (closing after around 5000 h of irradiation), which contributes to higher predicted temperatures compared to GERMINAL. Apart from rapid gap re-openings due to pin structure relaxation caused by power shutdown, the gap keeps always closed from the second power cycle on. TRANSURANUS is currently not equipped with a model accounting for JOG formation and evolution in the gap of fast reactor pins.

3.1.3.2 Post-INSPYRE results

Using the GERMINAL post-INSPYRE version, the P2CG size is only modified after the formation of JOG. This difference can be attributed to a lower Caesium release associated to the Xe, Kr release assessment given by the SCIANTIX model.

The differences in the TRANSURANUS predictions on the gap size brought about by the novel INSPYRE models are significant only at beginning of irradiation. The gap closure is slowed down after the initial start-up power increase (the fastest gap closure is obtained switching off the fuel grain growth and

employing the conservative correlation for cladding swelling). From the second power cycle on, there is no effect of gap re-opening caused by the models herein considered.

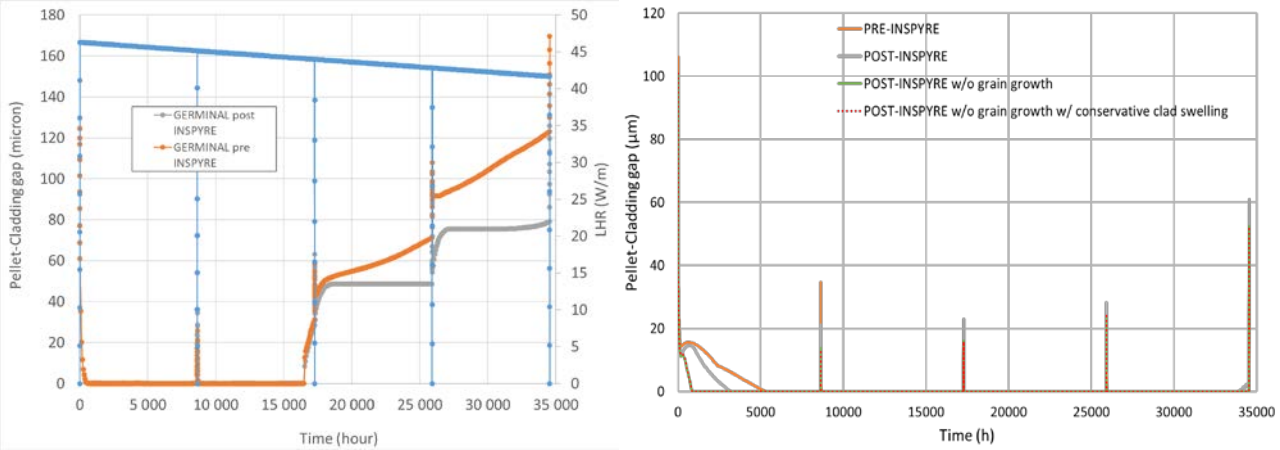

Figure 6: Pellet-Cladding Gap evolution at the Peak Power Node, as predicted by GERMINAL (left) and TRANSURANUS (right).

3.1.4 Cladding External Radius

3.1.4.1 Pre-INSPYRE results

In GERMINAL results, the cladding external radius (CER) increases slightly during the first two cycles due the irradiation creep under the internal pressure loading. After the second cycle, the CER increases faster under the supplementary effect of the cladding swelling induced by the fast neutron fluence.

TRANSURANUS predicts a more pronounced increase of the cladding outer radius, reaching slightly more than 5 mm, mainly due to an enhanced Pellet-Cladding Mechanical Interaction (PCMI, corresponding to a higher contact pressure as shown axially at the end of irradiation in Figure 18) with respect to GERMINAL predictions. Also, the swelling correlation employed by TRANSURANUS for 15-15Ti cladding material [13] predicts higher swelling rates compared to GERMINAL one (as demonstrated by Figure 15, showing the clad swelling axial profiles at the end of irradiation). The evolution of the cladding outer radius starts from the second irradiation cycle on, and is predicted as smooth, without sudden variations apart those caused by cycle transitions.

3.1.4.2 Post-INSPYRE results

For GERMINAL the post-INSPYRE results are similar to the reference ones, small differences observed for the cladding diameter are linked to pellet cladding interaction occurring with the gaseous swelling assessed by the SCIANTIX fission gas model.

The effect of INSPYRE models on the cladding outer radius evolution predicted by TRANSURANUS is stronger, compared to GERMINAL. The clad radial dimension is slightly higher, following the same dynamics along the irradiation cycles. The results of the sensitivity analyses, both switching off the fuel grain growth model and employing the conservative cladding swelling correlation, correspond to a much faster increase of the cladding radius up to sensibly higher predicted values (i.e., ~ 5.4 mm instead of ~ 5 mm). This is mainly due to an enhanced fuel-cladding interaction caused by a stronger fuel thermal expansion after the first power rise and a higher fuel gaseous swelling. Hence, a faster gap closure occurs (Figure 6), which determines higher contact pressures already from the first power cycle (~ 43 MPa in the "POST-INSPYRE" case, ~ 52 MPa switching off the fuel grain growth mechanism).

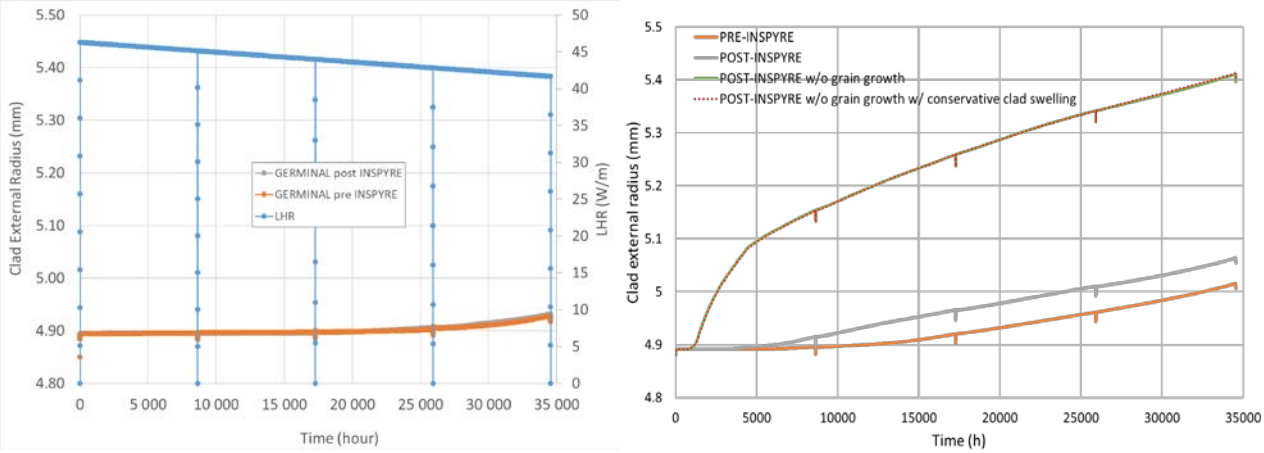

Figure 7: Cladding External Radius evolution at the Peak Power Node, as predicted by GERMINAL (left) and TRANSURANUS (right).

3.1.5 Fuel Pin Internal Pressure and Fission Gas Release

3.1.5.1 Pre-INSPYRE results

In GERMINAL results, the fuel pin internal pressure (FPIP) increases progressively as the fission gas release (FGR) leads to an accumulation of gases in the fuel pin internal volume. The pressure at the end of the fourth cycle is equal to 2.8 MPa with a FGR equal to 75%.

TRANSURANUS results show a much lower pin internal pressure (in the fuel-cladding gap, Figure 8), although the evolution along irradiation is similar between TRANSURANUS and GERMINAL (i.e., both progressively increasing following the power cycles). The predicted maximum value reached at the end of irradiation (before the final reactor shutdown) is around 1.25 MPa, which is lower than the typical EOL values predicted for FR pins (e.g., the INSPYRE irradiation experiments [14]), probably due to e.g., the axially heterogeneous composition of the ASTRID fuel column, featuring two fertile zones. The pin pressure dynamics is strictly related to the integral FGR evolution (Figure 9), which according to TRANSURANUS features a rapid increase during the initial phases of the first irradiation cycle, followed by a stabilization at around 30%. An additional sensitivity is here performed, consisting in switching on the TRANSURANUS model for burst releases of fission gases during operational power transients. The simulation of the additional burst release proves to have very little effect both on the pin internal pressure and on the FGR, as shown by the orange curves (full and dashed) in Figures 8 and 9.

3.1.5.2 Post-INSPYRE results

For GERMINAL the post-INSPYRE results are significantly different from the reference results specially regarding the FGR kinetics during irradiation. The SCIANTIX fission gas model leads a lower FGR rate during the nominal power periods and to sudden FGR bursts during the power down between cycles. These differences for FGR have a direct impact on the FPIP with some pressure jump between cycles.

The TRANSURANUS “POST-INSPYRE” simulation provides a much lower pin internal pressure and integral FGR (maximum values around 0.8 MPa and 14%, respectively). The reason for these dumped fission gas-related results is identified in the fuel grain growth model [15]–[17], which is currently tailored for LWR irradiation conditions and does not feature an upper limit for the grain size. The application of the present model to fast reactor irradiation conditions hence prevents a FGR typical of FR pins. This supported the need of performing a sensitivity analysis on the fuel grain growth model, whose results are also shown in the previous (and following) figures.

The green curves of Figures 8 and 9 show how both results are higher (approaching the pre-INSPYRE ones, all along the irradiation history) switching off the grain growth model in the post-INSPYRE simulation. On the contrary, the conservative correlation for cladding swelling [13] has no effect on the results obtained without considering grain growth. The sensitivity on the fission gas burst release model was again tested on the pressure and FGR results, activating here the SCIANTIX burst release model [17], [18]. The effect consists in sudden step increases of both pin pressure and FGR, similar to those observed also from GERMINAL simulations, leading to final values comparable to the ones obtained without possibility of fuel grain growth (i.e., pin pressure around 1.2 MPa and FGR around 25%). The simulation results show strong differences in both the pin pressure in the gap and the FGR. Therefore, open questions remain concerning the safety assessment of this heterogeneous FR pin for irradiation in the ASTRID reactor using the current versions of the codes. Developments are in particular needed in the coupling strategy between the codes and the SCIANTIX fission gas behaviour module.

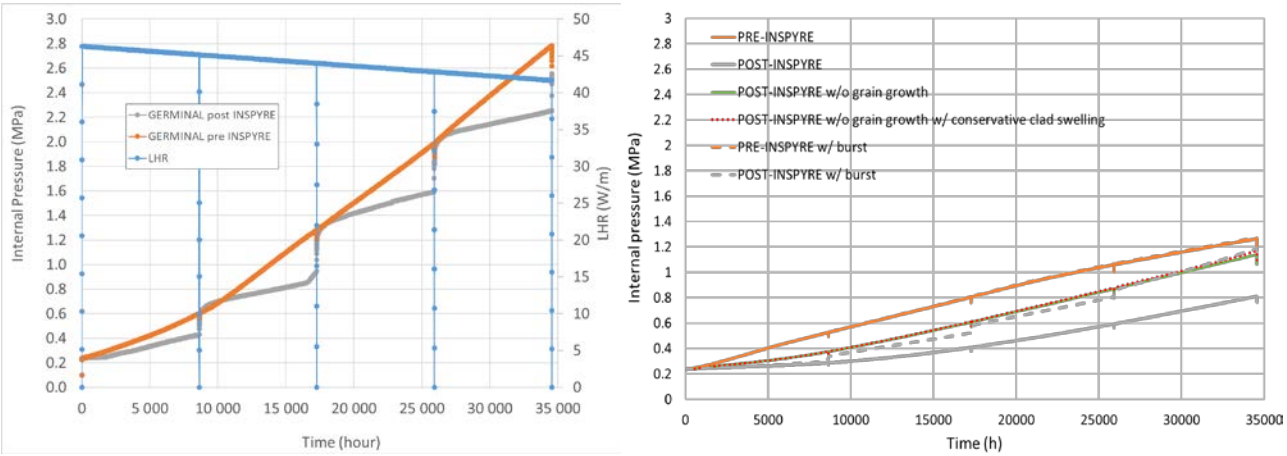

Figure 8: Fuel Pin Internal Pressure evolution as predicted by GERMINAL (left) and TRANSURANUS (right).

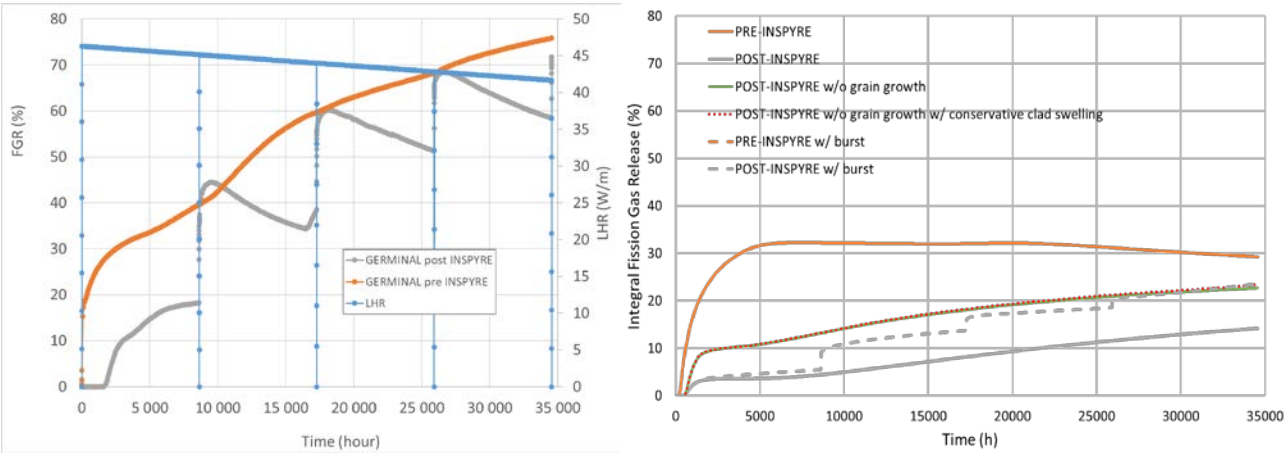

Figure 9: Fission Gas Release evolution at the Peak Power Node, as predicted by GERMINAL (left) and TRANSURANUS (right).

3.2 Axial profile results

3.2.1 Clad External Temperature and Fuel Central Temperature

3.2.1.1 Pre-INSPYRE results

For both codes, the clad external temperature (CET) and Fuel Central Temperature (FCT) axial distributions are correlated to the heterogeneous axial linear power with a mixed fissile-fertile fuel column. The CET increases from the bottom to the top with a slope proportional to the local linear power along the axial direction. The FCT evolution results from the sum of the CET and the thermal radial gradient, which is proportional to the local axial linear power.

3.2.1.2 Post-INSPYRE results

For both GERMINAL and TRANSURANUS, the CET is not modified by the post-INSPYRE options as it depends only on the linear power and on the heat power evacuation prescribed by the sodium coolant (imposed constant inlet temperature and mass flow rate as boundary conditions). For the FCT in GERMINAL there are some small differences between the pre- and the post-INSPYRE results, linked to the SCIANTIX fission gas model as it was commented in Section 3.1.1 for the peak power node results.

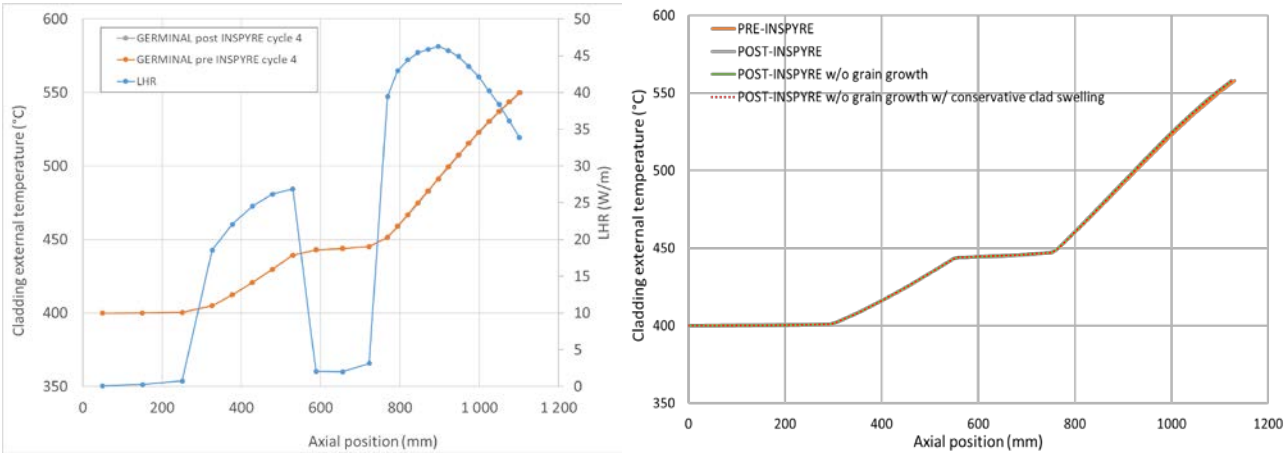

Figure 10: Axial profile of the Clad External Temperature at the end of cycle 4, as predicted by GERMINAL (left) and TRANSURANUS (right).

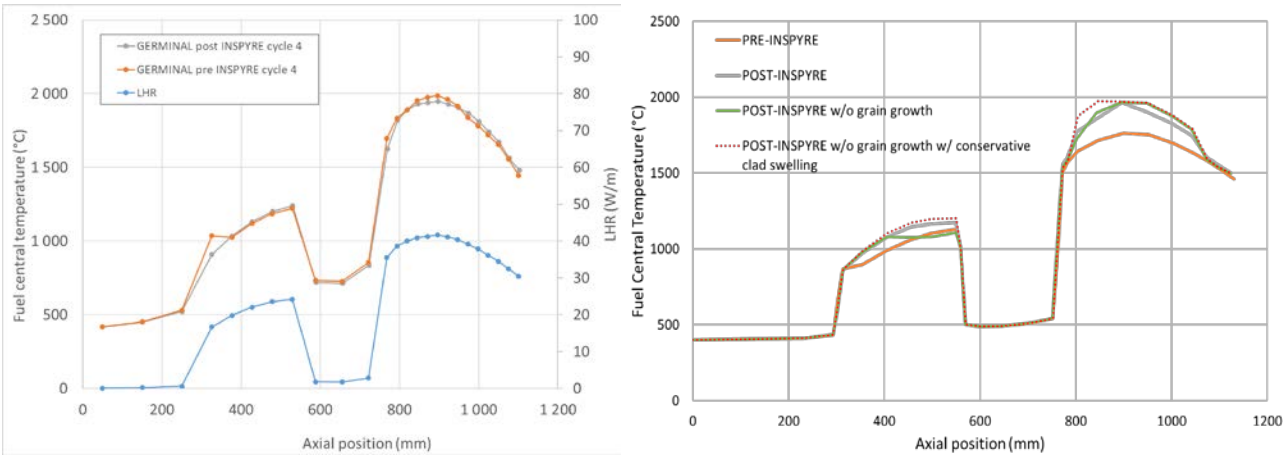

Figure 11: Axial profile of the Fuel Central Temperature at the end of cycle 4, as predicted by GERMINAL (left) and TRANSURANUS (right).

The novel INSPYRE models, on the other hand, determine a significant change of the FCT predicted by TRANSURANUS, confirming the impact of the change in fuel thermal properties (see Fig. 4). The effect

of the SCIANTIX module coupled to TRANSURANUS is dependent on the modelling of fuel grain growth. If no grain growth is considered, smaller fuel grains imply higher diffusivity of fission gases, and hence more fission gas release. This results in slightly higher fuel temperatures caused by lower gap conductance.

3.2.2 Fuel Pellet Inner Radius

3.2.2.1 Pre-INSPYRE results

For both codes the initial FPIR of the annular fissile pellets increases only in the upper fissile column. The FPIR increase assessed by GERMINAL is higher than the one predicted by TRANSURANUS (1.62 and 1.44 mm maximum values, respectively).

3.2.2.2 Post-INSPYRE results

For GERMINAL the post-INSPYRE options lead to a smaller FPIR extension in the upper fissile column. This effect has been commented in the peak power node section and can be attributed to the effect of the gaseous swelling.

The post-INSPYRE impact on TRANSURANUS is more visible in the higher top fissile region of the fuel pin (Fig. 12). The result obtained without the grain growth model active allows identifying the main cause of the difference in the higher fission gas release, namely retention of fission gas implies less gap pollution and hence milder fuel temperature, resulting in less extended restructuring.

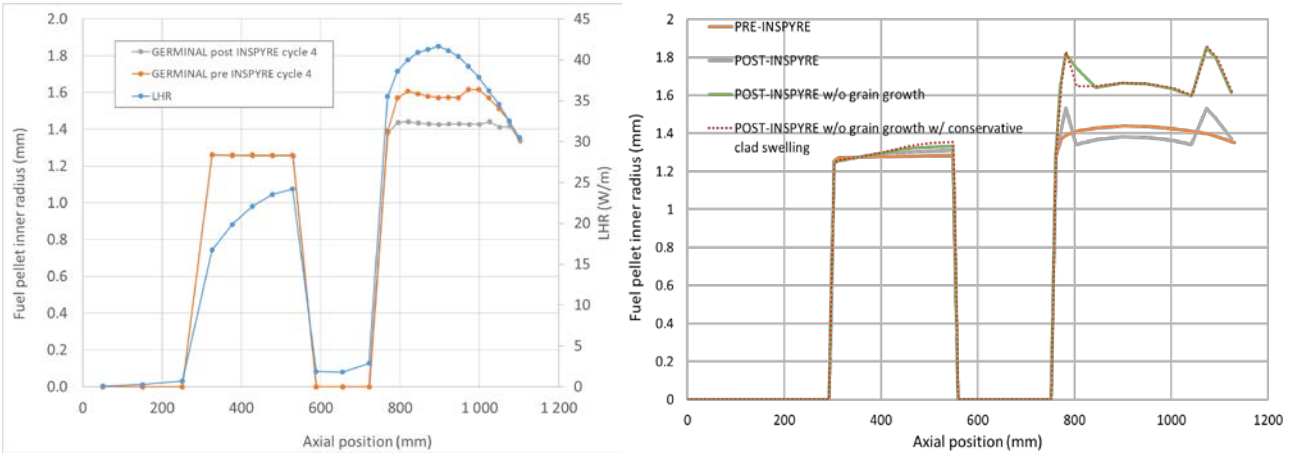

Figure 12: Axial profile of the Fuel Pellet Inner Radius at the end of cycle 4, as predicted by GERMINAL (left) and TRANSURANUS (right).

3.2.3 Pellet-To-Cladding Gap and Cladding Swelling

3.2.3.1 Pre-INSPYRE results

For both codes the P2CG at the beginning of cycle 1 is driven by the linear power profile with a gap approximately 20 microns greater in GERMINAL than in TRANSURANUS. In GERMINAL, at the end of cycle 4, the P2CG is open for the upper fissile column due to the presence of JOG between the pellet and the cladding, as explained in Section 3.1.3.

For GERMINAL, the cladding swelling (CS) profile at the end of cycle 4 leads to a maximal value located near the bottom of the upper fissile column. This axial position of the maximal value is consistent with an optimum damage rate based on the production rate induced by the dose and an annealing rate induced by the temperature. The TRANSURANUS CS profile seems to be driven mainly by the dose with

an axial position consistent with the power profile. TRANSURANUS yields a cladding swelling maximal magnitude three times larger than GERMINAL (5.5% and 1.67%, respectively).

3.2.3.2 Post-INSPYRE results

For GERMINAL the only difference with the post-INSPYRE results are for the P2CG and it is linked to the JOG thickness assessment modified by the inert gas model of SCIANTIX, as described in Section 3.1.3.

The post-INSPYRE TRANSURANUS results for pellet-to-cladding gap at the beginning of the 1st cycle (Fig. 13), coherently with those reported in Fig. 6, are mildly affected by the models introduced in the code, the gap thickness essentially resembling the axial power profile as they are driven by the fuel and cladding relative thermal expansion. The situation is more complex at the end of the 4th cycle (Fig. 14) where we observe that the gap is closed in the upper fissile zone of the pin while it is partially open in the lower fissile zone. Compared to the pre-INSPYRE results, the post-INSPYRE ones show a generally wider gap, which is coherent with the predicted fuel temperatures. As for the cladding swelling at the end of the 4th cycle (Fig. 15), it is worth noticing that TRANSURANUS predicts the peak of swelling in the lower part of the upper fissile zone if the conservative correlation for this property is considered.

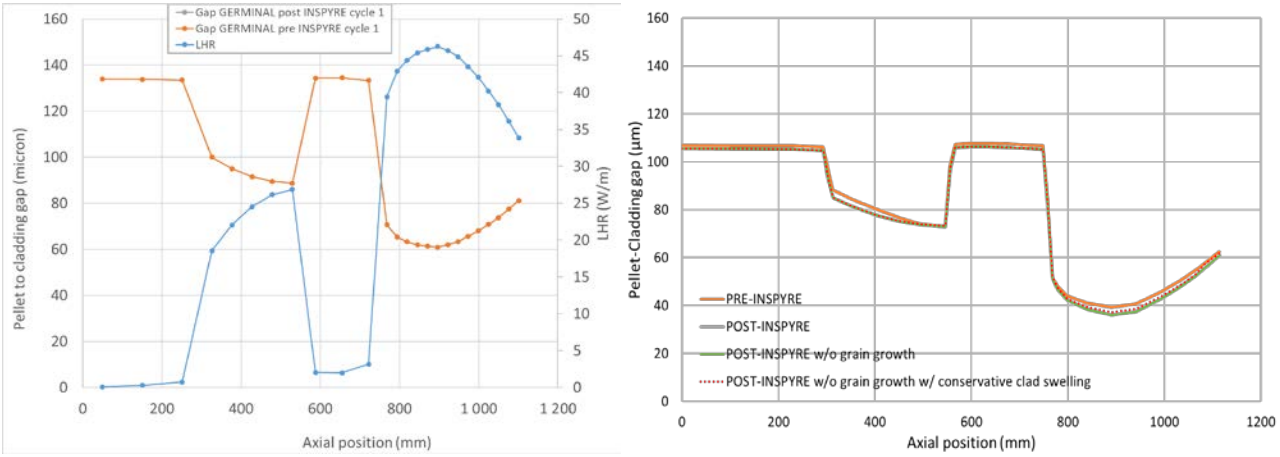

Figure 13: Axial profile of the Pellet-Cladding Gap at the beginning of cycle 1, as predicted by GERMINAL (left) and TRANSURANUS (right).

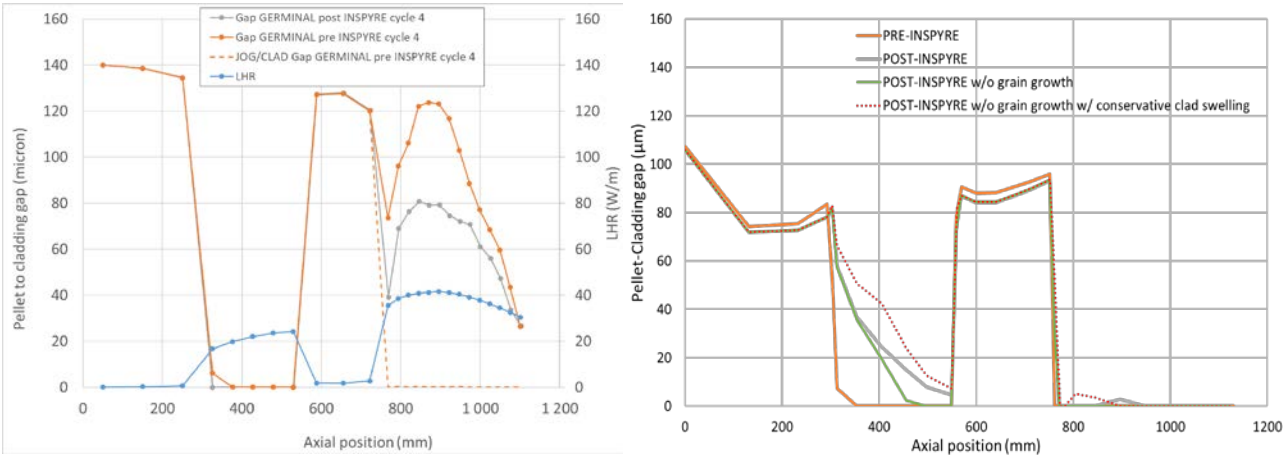

Figure 14: Axial profile of the Pellet-Cladding Gap at the end of cycle 4, as predicted by GERMINAL (left) and TRANSURANUS (right).

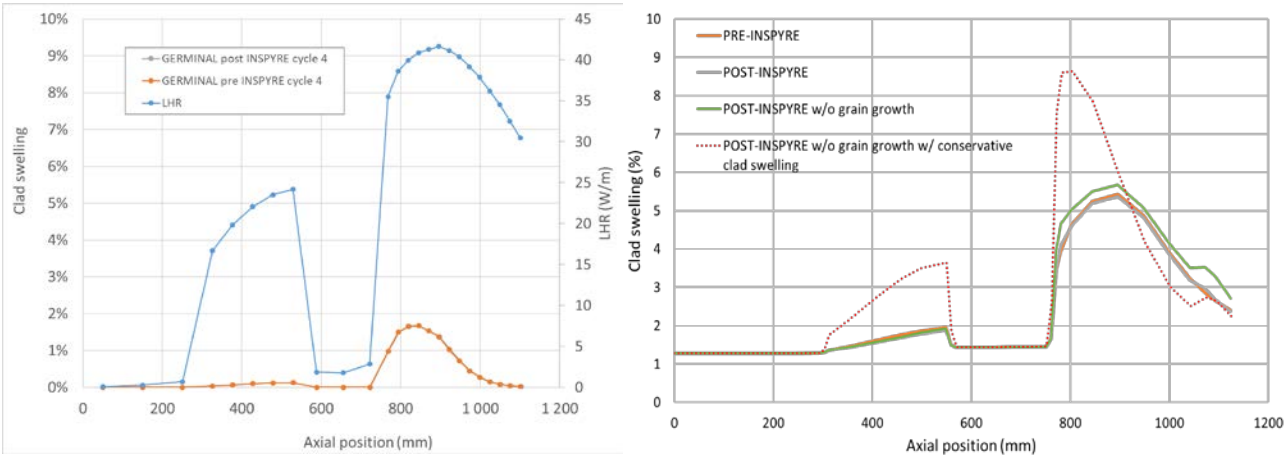

Figure 15: Axial profile of the Cladding Swelling at the end of cycle 4, as predicted by GERMINAL (left) and TRANSURANUS (right).

This is due to a combination of high fast neutron fluence and a cladding temperature in the critical range. Otherwise, the peak swelling corresponds to the axial region around the peak power node. This significant difference in the predicted cladding swelling behaviour deserves a discussion on the impact of this local deformation on the stress in the cladding, presented in the following section. The cladding swelling predicted by TRANSURANUS is substantially higher than the one calculated by GERMINAL (Figure 7). Nevertheless, the same axial shape of the volumetric swelling at EOL suggests a deeper investigation of the dependences of the GERMINAL and TRANSURANUS models on the cladding damage (dpa) or the neutron fluence. Finally, it is worth noticing that the conservative correlation gives the same swelling value at the peak power node, which explains why the TRANSURANUS results in time at that axial location (shown in the previous section) prove unaffected by the choice of a different swelling law.

3.2.4 Cladding Hoop Membrane/Bending Stress and Contact Pressure

3.2.4.1 Pre-INSPYRE results

In GERMINAL the cladding hoop membrane stress (CHMS) is almost constant along the z axis and the value of 21 MPa corresponds to the effect of the internal pressure at the end of cycle 4. The bending stress (CHBS) driven by the thermal and irradiation-swelling gradients in the cladding thickness exhibits a variation along the z axis consistent with the linear power profile. The fact that the CHBS has a nonlinear proportionality to the linear power seems to indicate that there is a significant contribution of the irradiation-swelling gradient.

3.2.4.2 Post-INSPYRE results

The main impact of the post-INSPYRE options for the GERMINAL results concerns the CHMS, which exhibits a small decrease for axial positions between 0 and 900 mm (2.2 to 1.7 MPa with pre and post options, respectively), and a significant increase on the upper part of the upper fissile column (2.2 to 53 MPa with pre- and post-INSPYRE options, respectively). These differences are due: on the one hand to a lower fuel pin internal pressure, leading to a CHMS of 1.7 MPa for axial positions where the pellet volume expansion accommodation is possible, and on the other hand to a pellet-cladding mechanical interaction leading to a maximal CHMS of 53 MPa at the top of the fissile column. The increase of the pellet-cladding mechanical interaction, confirmed by the contact pressure plotted in Fig. 18, can be explained by the contribution of the gaseous swelling in the post-INSPYRE results as commented in Section 3.1.4 for the cladding external radius.

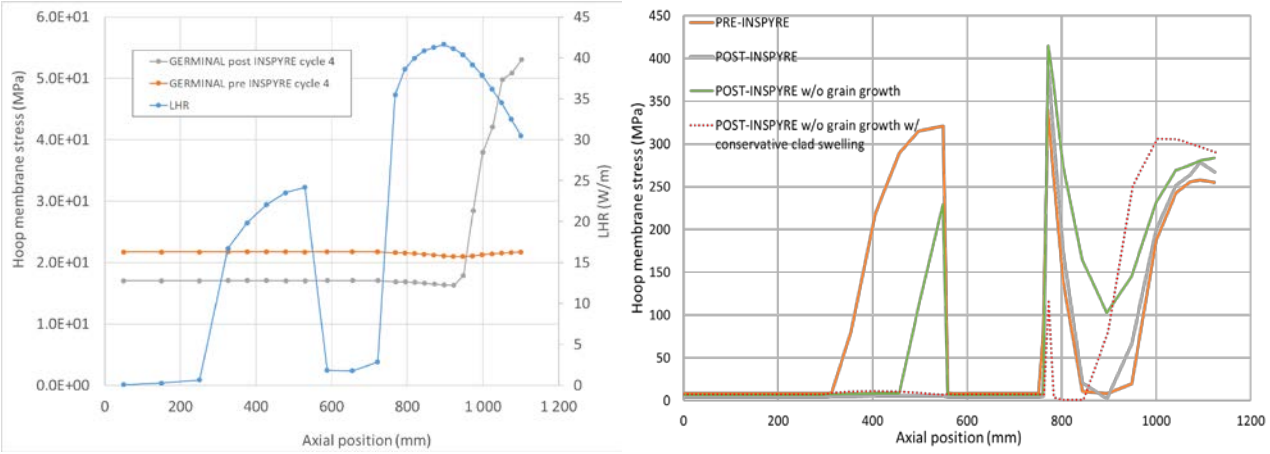

Figure 16: Axial profile of the Cladding Hoop Membrane Stress at the end of cycle 4, as predicted by GERMINAL (left) and TRANSURANUS (right). Please, note the scale difference.

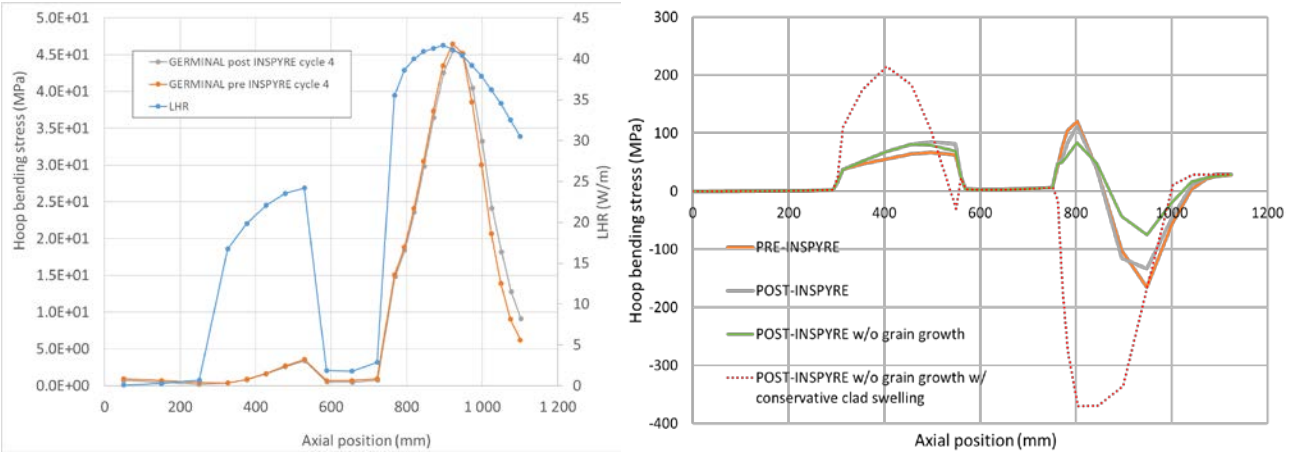

Figure 17: Axial profile of the Cladding Hoop Bending Stress at the end of cycle 4, as predicted by GERMINAL (left) and TRANSURANUS (right). Please, note the scale difference.

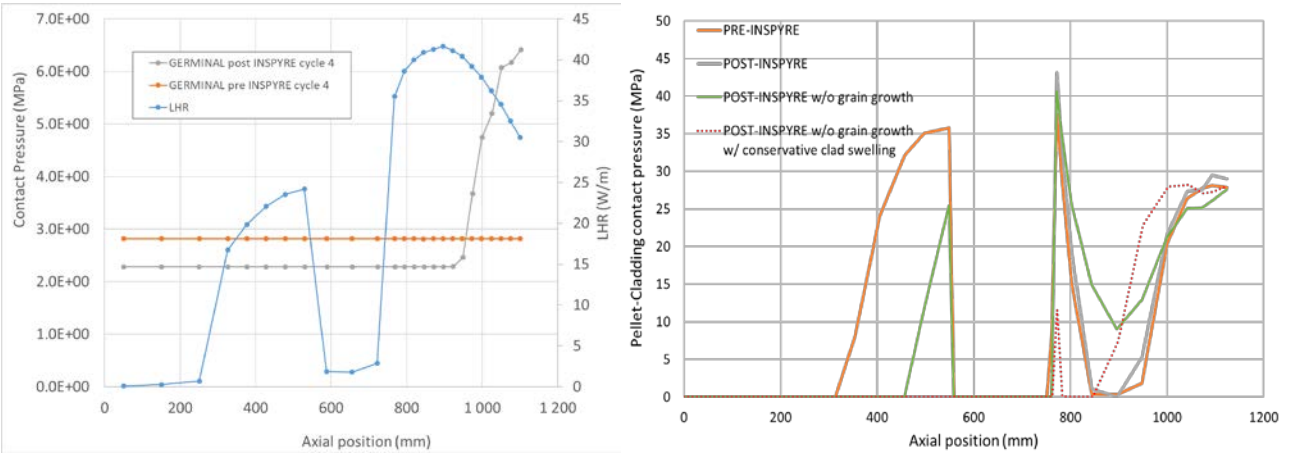

Figure 18: Axial profile of the Pellet-Cladding Contact Pressure at the end of cycle 4, as predicted by GERMINAL (left) and TRANSURANUS (right). Please, note the scale difference.

The results of TRANSURANUS are influenced by several modelling hypotheses:

- Relocation recovery is not considered, implying generally high levels of contact pressure between fuel and cladding (Fig. 18).
- Strong axial variations of cladding swelling contribute to stress concentrations between the fertile and fissile zones of the fuel pin (see the impact of considering a conservative clad swelling correlation in Figs. 16-18).

It should be noted that for both codes, the stress levels presented in this section indicate the right order of magnitude but do not constitute accurate estimations. They should therefore only be used for a qualitative analysis. One should in particular be careful in deriving strong conclusions from these stress values and avoid comparing them directly with design limits.

4 DISCUSSION

This section discusses for each code the lessons learned from the comparison between pre- and post-INSPYRE code versions, as well as the global impact of the post-INSPYRE results.

4.1 GERMINAL

For GERMINAL the main aspect to consider regarding the impact of the post-INSPYRE options concerns the pellet-cladding mechanical interaction loading. If we refer to pre-INSPYRE results, stresses induced by pellet-cladding interaction are negligible up to the end of life. This conclusion is associated to some assumptions, such as the possibility of a complete accommodation of the relocation displacement in case of closed gap (this possibility delaying a strong interaction between pellet and clad until the accommodation is complete). Another assumption reducing the pellet-cladding interaction consists in neglecting the contribution of the gaseous swelling. Both assumptions have been verified thanks to the code validation on a large experimental database. In the case of the post-INSPYRE results, we can observe that an increase of the gaseous swelling contribution leads to reach a complete relocation accommodation and then to trigger pellet-cladding interaction. Therefore, this result draws our attention to the fact that a predictive assessment of the fuel pin behaviour outside of the validation database is not yet possible if we consider the risk of error compensation between fuel models with remaining empirical parameters or formulations. For a predictive assessment of the pellet-cladding mechanical interaction, improvements are needed with a more physically based fission gas modelling and with a 3D simulation of the fuel pin multi-physics behaviour under irradiation.

4.2 TRANSURANUS

For TRANSURANUS, the main improvement emerging in this benchmark exercise is related to the implementation of updated thermal properties. The impact on fuel temperatures predictions is significant and, besides not having shown in this deliverable any comparison with experimental data, it is safe to claim that the availability in the code of more up to date and comprehensive correlations is beneficial for the application of TRANSURANUS. As for the predictions of mechanical stress in the cladding because of PCMI, the difference between TRANSURANUS and GERMINAL calls for attention in drawing conclusions. The two codes present a different treatment of the recovery of relocation, with GERMINAL considering an accommodation process associated to the relocation strain (see the description in Section 4.1) while TRANSURANUS does not consider any recovery. Lastly, the coupling of

TRANSURANUS with SCIANTIX showed that the inclusion of a physics-based model for fission gas behaviour modelling is feasible, robust and reliable, and considerably influences the predictive capabilities of the code. Nevertheless, this benchmark exercise allowed identifying some limitations of the current coupling, highlighting e.g., the need of further development of a coherent grain growth model to be applied in fast reactor conditions.

5 CONCLUSIONS

A benchmark between GERMINAL and TRANSURANUS was proposed and performed on the ASTRID case study considering an axially heterogeneous fuel pin featuring fertile and fissile zones. The simulation results were presented for both codes in their pre- and a post-INSPYRE versions (i.e., employing the novel models developed in the framework of INSPYRE, as defined in Deliverable D7.2 [1]).

The discussion of the results concerns the main physical aspects affecting two important engineering design criteria: the power-to-melt and the cladding maximal hoop stress. The results yielded by both pre-INSPYRE and post-INSPYRE of the two codes were compared while highlighting the differences between the codes. In addition, the last section summarizes the lessons learned for each code as well as open points for future developments and improvements. This is fundamental for the continuous development of fuel performance codes targeting the pin performance in fast reactor and Generation IV irradiation conditions.

REFERENCES

[1] P. Van Uffelen *et al.*, "Incorporation and verification of models and properties in fuel performance codes," *INSPYRE, D7.2 version 1, 2020*.

[2] L. Luzzi *et al.*, "Definition of detailed configurations of the case studies for the fuel performance simulations in Task 7.3," *INSPYRE, MS16 version 1, 2019*.

[3] C. Venard, "The ASTRID core at the end of the conceptual design phase," 2017.

[4] G. Khvostov, K. Mikityuk, and M. A. Zimmermann, "A model for fission gas release and gaseous swelling of the uranium dioxide fuel coupled with the FALCON code," *Nucl. Eng. Des.*, vol. 241, no. 8, pp. 2983–3007, 2011.

[5] B. Faure, P. Archier, J.-F. Vidal, J. M. Palau, and L. Buiron, "Neutronic calculation of an axially heterogeneous ASTRID fuel assembly with APOLLO3®: Analysis of biases and foreseen improvements," *Ann. Nucl. Energy*, vol. 115, pp. 88–104, 2018.

[6] T. Beck *et al.*, "Conceptual design of ASTRID fuel sub-assemblies', Nuclear Engineering and Design," *Nucl. Eng. Des.*, vol. 315, pp. 51–60, 2017.

[7] A. Magni *et al.*, "Modelling and assessment of thermal conductivity and melting behaviour of MOX fuel for fast reactor applications," *J. Nucl. Mater.*, vol. 541, p. 152410, 2020.

[8] A. Magni *et al.*, "Report on the improved models of melting temperature and thermal conductivity for MOX fuels and JOG," *INSPYRE, D6.2 version 2, 2020*.

[9] S. Lemehov, "New correlations of thermal expansion and Young's modulus based on existing literature and new data," *INSPYRE, D6.3 version 1, 2020*.

[10] D. Pizzocri *et al.*, "Review of available models and progress on the sub-models dealing with the intra- and intergranular inert gas behaviour," *INSPYRE, D6.1 version 1, 2019*.

[11] K. Lassmann, "TRANSURANUS: a fuel rod analysis code ready for use," *J. Nucl. Mater.*, vol. 188, no. C, pp. 295–302, 1992, doi: 10.1016/0022-3115(92)90487-6.

[12] Y. Philipponneau, "Thermal conductivity of (U, Pu)O_{2-x} mixed oxide fuel," *J. Nucl. Mater.*, vol. 188, pp. 194–197, Jun. 1992, doi: 10.1016/0022-3115(92)90470-6.

[13] L. Luzzi, A. Cammi, V. Di Marcello, S. Lorenzi, D. Pizzocri, and P. Van Uffelen, "Application of the TRANSURANUS code for the fuel pin design process of the ALFRED reactor," *Nucl. Eng. Des.*, vol. 277, pp. 173–187, 2014, doi: 10.1016/j.nucengdes.2014.06.032.

[14] B. Boer *et al.*, "Report describing the results of the benchmark between improved codes and previous versions on selected experimental cases," 2020.

[15] J. B. Ainscough, B. W. Oldfield, and J. O. Ware, "Isothermal grain growth kinetics in sintered UO_2 pellets," *J. Nucl. Mater.*, vol. 49, no. 2, pp. 117–128, Dec. 1973, doi: 10.1016/0022-3115(73)90001-9.

[16] P. Van Uffelen *et al.*, "An experimental study of grain growth in mixed oxide samples with various microstructures and plutonium concentrations," *J. Nucl. Mater.*, vol. 434, no. 1–3, pp. 287–290, 2013, doi: 10.1016/j.jnucmat.2012.11.053.

[17] D. Pizzocri, T. Barani, and L. Luzzi, "SCIANTIX: A new open source multi-scale code for fission gas behaviour modelling designed for nuclear fuel performance codes," *J. Nucl. Mater.*, vol. 532, p. 152042, 2020.

[18] T. Barani *et al.*, "Analysis of transient fission gas behaviour in oxide fuel using BISON and TRANSURANUS," *J. Nucl. Mater.*, vol. 486, pp. 96–110, 2017, doi: 10.1016/j.jnucmat.2016.10.051.